ANALYTICAL BIOCHEMISTRY 202, 275–285 (1992)

Computer-Assisted Tracking of Actin Filament Motility

Steven S. Work and David M. Warshaw[1]
Department of Physiology & Biophysics, University of Vermont, Given Medical Building, Burlington, Vermont 05405

Received September 9, 1991

***In vitro* motility assays, in which fluorescently labeled actin filaments are propelled by myosin molecules adhered to a glass coverslip, require that actin filament velocity be determined. We have developed a computer-assisted filament tracking system that reduced the analysis time, minimized investigator bias, and provided greater accuracy in locating actin filaments in video images. The tracking routine successfully tracked filaments under experimental conditions where filament density, size, and extent of photobleaching varied dramatically. Videotaped images of actin filament motility were digitized and processed to enhance filament image contrast relative to background. Once processed, filament images were cross correlated between frames and a filament path was determined. The changes in filament centroid or center position between video frames were then used to calculate filament velocity. The tracking routine performance was evaluated and the sources of noise that contributed to errors in velocity were identified and quantified. Errors originated in algorithms for filament centroid determination and in the choice of sampling interval between video frames. With knowledge of these error sources, the investigator can maximize the accuracy of the velocity calculation through access to user-definable computer program parameters.**

Force production and shortening in muscle are believed to result from the cyclic interaction between the contractile proteins, myosin and actin, as the myosin hydrolyzes ATP. Until recently, this interaction was characterized mechanically through muscle fiber studies (1) or biochemically through interactions of isolated actin and myosin in solution (2). Recently, an *in vitro* motility assay in which a single fluorescently labeled actin filament is propelled by just a few myosin molecules adhered to a glass coverslip has been developed (3,4). With the advent of image enhancement technologies and digital video microscopy, single-actin-filament motion can now be readily visualized.

In the motility assay, actin filament velocity is believed to be a mechanical expression of the actomyosin interaction and thus forms the basis for several hypotheses concerning this molecular transduction process (5–8). Specifically, actin filament velocity may be used to estimate the motion distance that a single myosin motor molecule imparts to actin per ATP hydrolyzed. Actin filaments are flexible structures that undulate in response to Brownian motion and other physical forces. In addition, visual noise generated in the recording system further reduces the accuracy in determining actin filament position. Since changes in actin filament position with time are used to calculate actin filament velocity, the accuracy of the methodology for locating actin filament position in such a noisy visual environment must be considered before actin filament velocity is determined as true myosin-derived filament sliding.

We have developed a computer-based actin filament tracking system to analyze low-light-level digitized video images of fluorescently labeled actin filaments being propelled by myosin. This system reduces investigator analysis time and removes as much investigator bias as possible. Although the algorithms are designed to track actin filaments, they can be applied to problems of general object tracking (e.g., sperm, bacterial, and cell motility) where video recording is the medium of choice and where objects remain in the focal plain of the microscope.

METHODS

In Vitro Motility Assay

The motility assay was performed as described previously (7). In brief, a nitrocellulose-coated coverslip and microscope slide were used to create a microtest chamber through which various test solutions were perfused. First, monomeric smooth or skeletal muscle myosin (250 μg/ml in 300 mM KCl buffer) was perfused into

[1] To whom reprint requests and software availability requests should be addressed.

0003-2697/92 $3.00

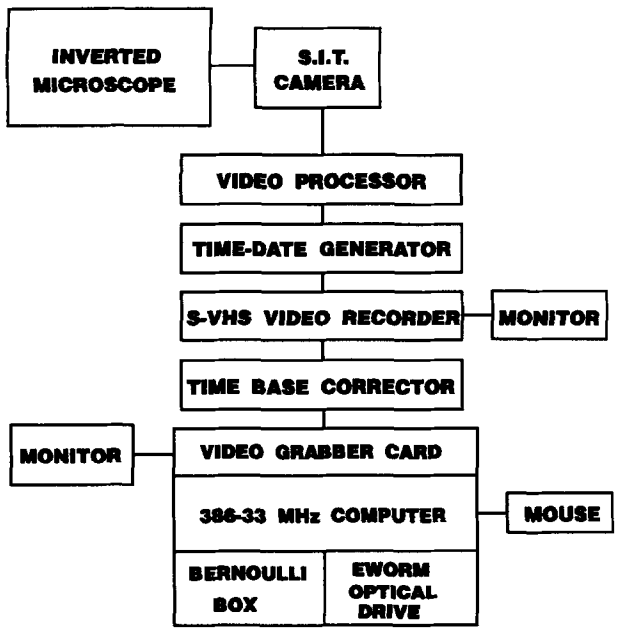

FIG. 1. Instrumentation block diagram. See text for details.

the chamber and allowed to adhere to the nitrocellulose surface. Then, bovine serum albumin in the 300 mM KCl buffer was flushed through to wash out unbound myosin and to coat any exposed nitrocellulose surfaces. Actin filaments that were previously labeled with fluorescent tetramethylrhodamine–phalloidin were introduced into the flow cell in an ATP-free low-salt buffer (25 mM KCl) and allowed to bind to the myosin. After unbound actin filaments were flushed out with the ATP-free buffer, low-salt buffer containing 1 mM ATP and 0.5% methylcellulose was perfused through the chamber to initiate actin filament motion.

Recording Actin Filament Movement

Actin filament motion was observed through an inverted microscope (Zeiss, IM-35) equipped for epifluorescence (see Fig. 1). Video images, obtained through an image-intensified video camera (Dage, 66 SIT), were corrected for uneven field illumination by background subtraction using a dedicated digital image processor (Hamamatsu, Argus 10). The processed image was fed into a time–date generator (Panasonic, WJ-810) to superimpose the elapsed experiment time on the video image. These images were recorded on sVHS video tape (Panasonic, AG-7400) for filament velocity analysis at a later time. The real time image was monitored through the video recorder.

The recorded images were digitized by playback through a time base corrector (ForA, 210) to guarantee strong synchronization signals for the video grabber card (Coreco, Oculus 300). The computer-based video digitizing system consists of a 33-MHz 386 personal computer (Gateway 2000) running under DOS 4.0 (Microsoft), video grabber card, two external mass data storage systems (Bernoulli Box, 44 Mbytes/cartridge; Data Storage Systems, EWORM optical drive, 600 Mbytes/cartridge), and a serial mouse (Mouse Systems Corp.).

The video grabber card digitized video frames into a 480 vertical by 512 horizontal pixel array with 8-bit pixel intensity (i.e., 256 possible gray levels). To draw boxes and characters over the digitized image, the video card used the most significant bit to create a "graphic plane," preserving only 7 bits of intensity information. A pixel gray level of 0 represents black, with 127 equaling white. The spatial resolution of the recording system was 192 nm/pixel using a 63× objective (Zeiss, Planapochromat, N.A. = 1.4).

Automated Filament Tracking Program

The basic operating principles of the filament tracking system are as follows. After identifying a video segment containing filament motility, the user initiates SWEEP, a program allowing the user to define a portion of the video image to be digitized, time between image grabs, and number of images to be grabbed (Fig. 2C) and finally to save these images to a mass storage device. The data are retrieved and analyzed using DECODE, a program that performs image enhancement, processing, and pattern recognition. For each image, DECODE generates a file that contains the location and description of each actin filament that was detected. This information is passed to a program, ANALYZE, that cross correlates objects in consecutive frames, thus identifying a filament's path of motion. Finally, a user interactive program (XVIEW) calculates filament velocity from the distance that the filament travels between consecutive frames.

These four programs (SWEEP, DECODE, ANALYZE, and XVIEW) are described in greater detail, with the image processing required to analyze actin filament motion emphasized, given that actin filament images vary in size, density, and extent of photobleaching (see Figs. 2A, 2B, and 2D).

All programs were written in Lattice C Version 3.1. Many of the algorithms rely on functions that exist within the subroutine library (Coreco, Gray Library), provided by the video grabber card manufacturer.

SWEEP—Video Snapshot Program

SWEEP allows the user to define a portion of the video frame that will be digitized by moving a box outline with the cursor keys over the desired image area (Fig. 2A). The box is 200 pixels in length by 150 pixels in height or 12% of the entire frame. Given these dimensions, the computer can store up to 16 box images in main memory. The user also defines the total number of

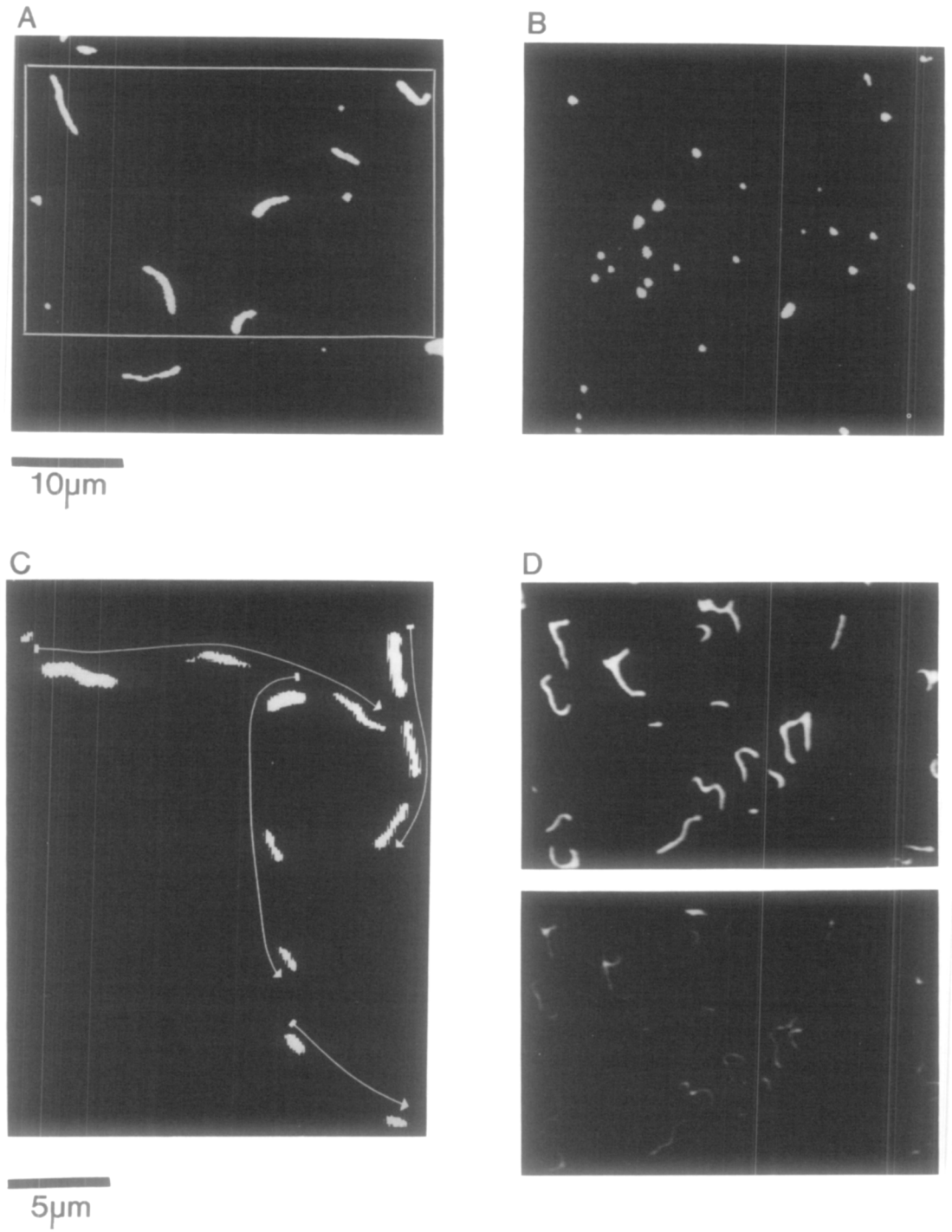

FIG. 2. Digitized video images of single actin filaments. (A) Actin filaments are seen within the box outline used by SWEEP to demarcate the image area to be digitized. Experimental conditions were phosphorylated smooth muscle myosin (250 μg/ml) in 60 mM KCl salt buffer with 1.0 mM MgATP at 30°C. (B) With phosphorylated smooth muscle myosin (250 μg/ml) in 25 mM KCl salt buffer with 0.025 mM MgATP and 30°C, the appearance of actin filaments can vary dramatically. Note how these small fragmented actin filaments are compared to the longer filaments in A. Magnification is the same as that of A. (C) Composite video image of three frames in which several actin filaments move within the visual field. The path and direction of motion are indicated by the solid white line and arrowhead. The time between video snapshots was 6.0 s. Experimental conditions are similar to those given for in A. (D) Video images of actin filaments interacting with phosphorylated smooth muscle myosin (50 μg/ml) in 25 mM KCl salt buffer with 1 mM MgATP at 30°C. Note the extent of photobleaching that can occur within 25 s. With appropriate oxygen scavengers and reducing agents, photobleaching can be greatly retarded (7). Magnification is the same as that of A.

box images and the time between grabs. The minimum time between grabs is 220 ms, which is limited by computer I/O. The user then positions the videotape at the desired location, sets the video recorder to continuous play, and triggers the program by a keystroke to begin digitizing video data. Once triggered, the computer grabs a box image and records both its location within the frame and its grab time, using the computer's clock as a reference. This is important, because given computer I/O, the time between grabs does not always exactly equal that requested by the user (see Fig. 8). After grabbing the desired number of images, the images are then written to a file on a mass storage device.

For high time resolution, a version of SWEEP that allows frame to frame digitization, giving 33 ms resolution, has been developed. (see Fig. 7). At present, this program requires that the user manually single frame advance through the desired segment of video tape and trigger the computer after each frame advance. This is a time-consuming process and we are currently developing an automated computer-controlled single-frame advance capability using the VCR's editing controller jack.

DECODE—Filament Detection Program

Background threshold gray level determination. The next step in the analysis is to determine the number of filaments per digitized image and their dimensional attributes. Prior to filament characterization, digitized images are filtered using a 3×3 convolution (Coreco, Gray Library subroutine: "GRLOW") to minimize recording system noise and processed to enhance filament contrast. A commonly used contrast enhancement technique is to alter the appearance of the background image by adjusting its gray level so that the differences in background and object gray levels are as great as possible. Therefore, a threshold background gray level value is chosen so pixels with gray levels equal to or less than the threshold value are set to zero (i.e., black). All other pixels retain their gray level. This gray level transformation defines a gray level lookup table. Since no clear distinction between background and filament gray levels exists (see Fig. 3, inset) an iterative process is used to determine the optimal threshold value.

The optimal threshold gray level determination begins by defining a gray level lookup table with a threshold value designated by the user. Once the image has been processed through the lookup table, pixels with gray levels greater than 0 are grouped along horizontal lines, with a group consisting of either a single pixel or a set of adjoining pixels. An object (i.e., actin filament) is formed by linking pixel groups from adjacent lines that have overlapping horizontal pixel positions (see Fig. 5, lower half of pixel map). Once formed, the object area (i.e., number of pixels) is determined and if smaller than a user-specified value (e.g., 3 pixels), the object is considered noise and ignored. Finally, the total number of objects is determined and compared to the number obtained using the previous threshold gray level value. If the object number changes by more than a user-definable value (usually 1), the threshold gray level is incremented and the procedures discussed above repeated until the appropriate threshold value is reached.

As an example, the results of this iterative process are shown in Fig. 3. In the original image (Fig. 3A), one can detect between 10 and 20 filaments by eye, although several are difficult to distinguish from background. At very low threshold gray values (0–14), almost all pixels have gray levels greater than the threshold (see Fig. 3, inset); therefore these pixels form a single object, giving the low object number. As the threshold value climbs to the range of the average background gray level (i.e., 15–22), the number of objects rapidly grows, most of which are considered noise. However, the number of remaining objects is still aberrantly high (>60 objects). With further increases in threshold value, the number of objects declines to a constant level of 11, until the number of objects declines even further when a threshold gray level of 45 is reached. The filament images tend to fade away at these high threshold values (Figs. 3E and 3F). Thus a threshold value is considered optimum when the object number versus threshold gray level relationship maintains a plateau (i.e., no change in object number) following threshold values that give abnormally high object counts.

The optimum threshold value is saved to speed the analysis for the next image. Since photobleaching does alter filament intensity (Fig. 2D), the optimum threshold value is reduced by a user-defined value before the threshold determination for the next box begins.

Filament centroid/center determination. Once the appropriate threshold is achieved and the number of objects identified, an object's dimensional attributes are calculated. These attributes are essential for tracking a filament between consecutive box images. Filament attributes are as follows: total pixel area, major axis length, minor axis length, major axis angular orientation, and centroid/center position with weighting for pixel intensity. The 5:4 horizontal to vertical pixel aspect ratio was accounted for in all dimensional calculations. Using floating point math, subpixel resolution is possible given that filament images span many pixels (9).

Changes in filament centroid position between box images are used to calculate filament velocity. The error in determining this position contributes to errors in estimating filament velocity. The centroid position is sensitive to image noise (Fig. 4), photobleaching, Brownian motion, and filament length (Fig. 5). The centroid is determined by weighting each pixel by its absolute gray level intensity. A more accurate weighting can be

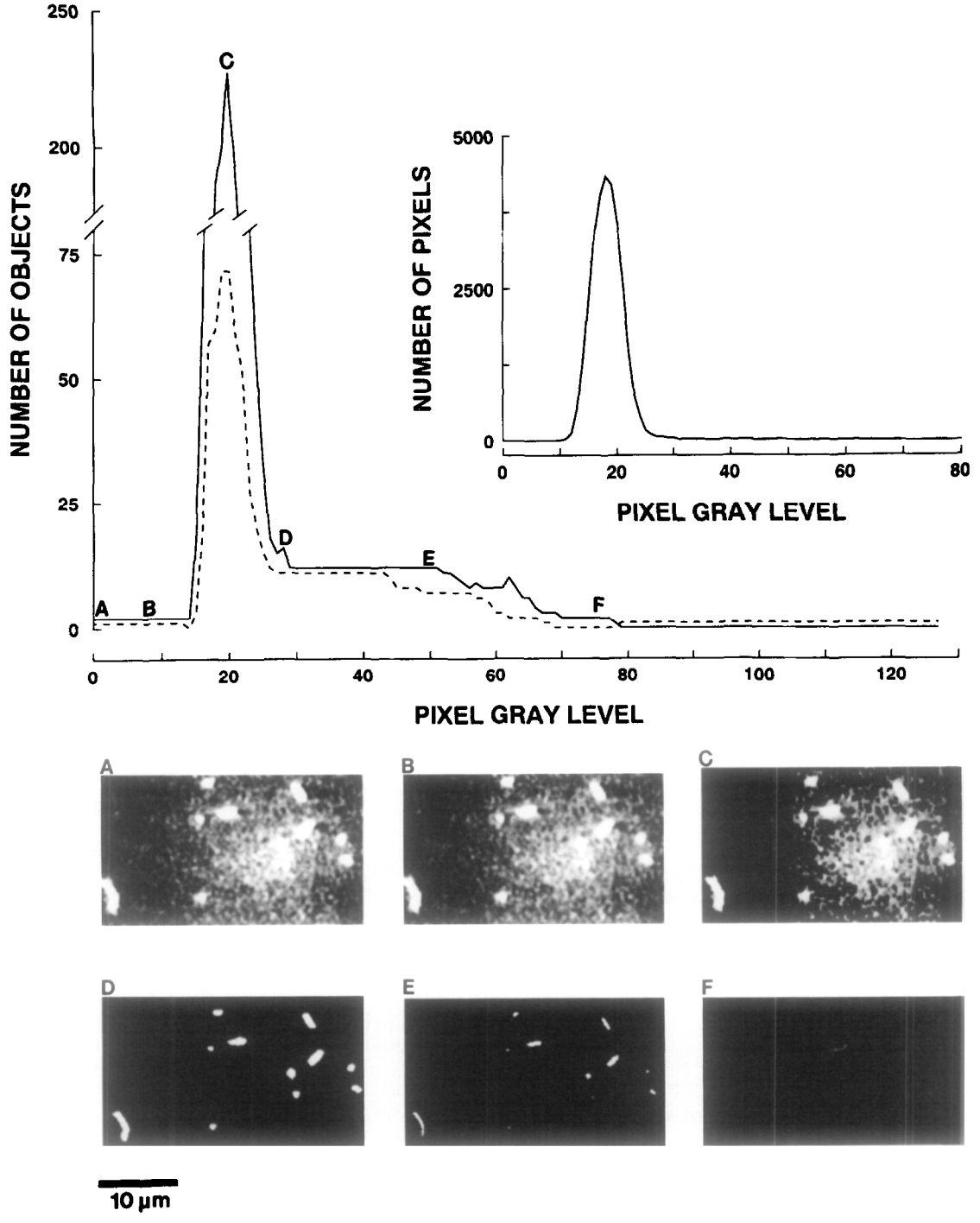

FIG. 3. Background threshold determination. The program DECODE improves filament to background contrast by determining an optimum background pixel gray level (see text for details). Plotted are the total number of objects (solid line) and the number of objects not considered noise (dashed line) as the background gray level threshold value varies between 0 and 127 for the original image A. An object (i.e., actin filament) is a contiguous group of pixels with gray levels above threshold. Images B–F are the result of image processing using the indicated threshold gray level. The inset is the pixel gray level histogram for image A prior to processing. Note that there is no clear demarcation between background and filament image gray levels.

achieved using the pixel intensity relative to the threshold background gray level. In either case, if the stoichiometry of fluorophore to actin is constant, then brighter pixels indicate a greater amount of actin (6) and give weight to where actin mass exists. For short filaments, this approach is sufficient, but for long filaments (i.e., >5 μm), which frequently bend, the centroid can be located off the filament. Any off-filament centroids would

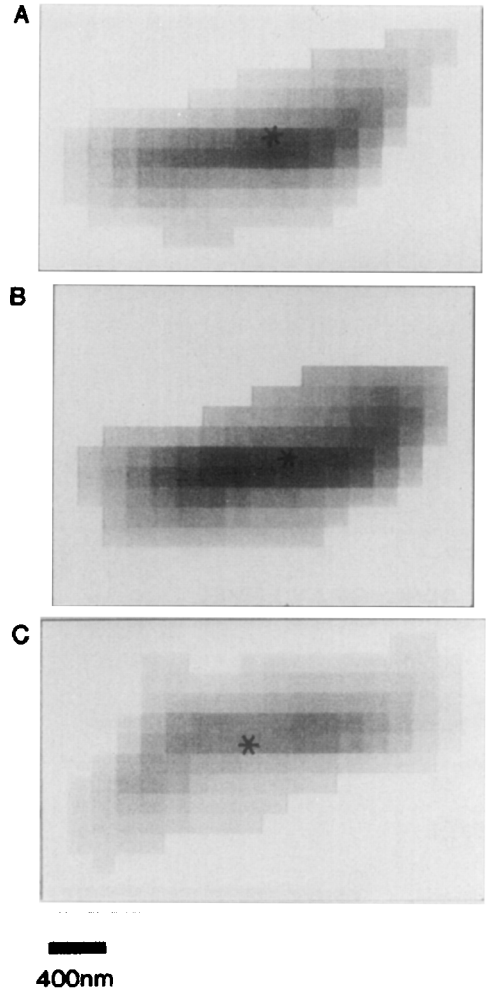

FIG. 4. Digitized actin filament image and centroid. A single digitized actin filament image in three consecutive video frames is shown. The image has been magnified sufficiently that individual pixels and their respective gray levels are discernible. Note that the outline of the filament changes dramatically between frames (i.e., 33 ms), as does the centroid position (*).

underestimate the true path length as a filament moves and thus generate significant velocity errors (see Fig. 5).

For experimental conditions where actin filaments are long, an alternate user-designated algorithm in which the filament center rather than its centroid is determined is chosen. The filament is rescanned along an angle that is closest to being perpendicular to the filament's major axis (see Fig. 5, upper half of pixel map). Due to the discrete pixel nature of the image, only four scan angles can be applied (0, 45, 90, 135°). Above threshold, pixel groups are formed along scan lines and a weighted centroid position is determined for each group. The filament endpoints are located by searching the pixel groups for any group having only one adjoining group. Beginning at each endpoint, a continuous path through as many group centroids as possible is determined. The longest path that contains the most pixel groups is considered the true filament length and half this distance is marked as the filament center.

In presenting the tracking capabilities of these algorithms, we chose to characterize filament motion from

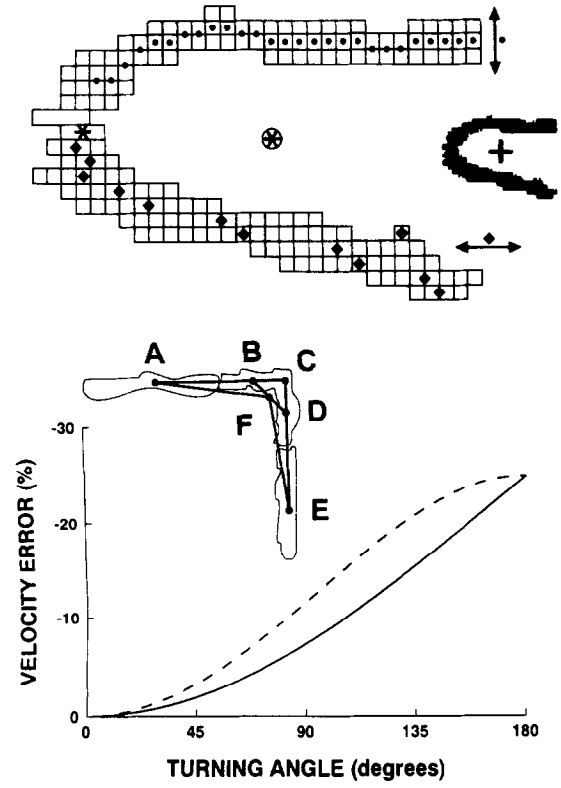

FIG. 5. Actin filament centroid/center determination. The upper illustration is the pixel map for the digitized video image seen to the right. The centroid for this highly curved actin filament is indicated by the cross in the actual image and the enclosed asterisk for the pixel map, whereas the filament center is indicated by an asterisk in the pixel map. The lower half of the pixel map shows the result of horizontal scans of the map with the centroid for pixel groups on a given scan line indicated by a diamond. In the upper half of the pixel map are centroids for pixel groups following vertical scanning of the map. The vertical scan would be used for this filament in order to calculate its center given that the filament's major axis lies closest to the horizontal. As described in the text, filament centers are determined for long filaments by scanning the filament image at an angle perpendicular to the major axis angle. The lower half of the figure is the result of a theoretical treatment to predict the extent to which actin filament velocity is underestimated if the filament turns at various angles (θ = $\sphericalangle$ ACE). One can simply calculate from geometrical considerations the difference by which the centroid (A, F, E) travels during a turn compared to the true filament center (A, C, E). Assume that a filament of length $L = AC = CE$ travels at a velocity equal to its length per unit time and that the filament is tracked for three time units. The true distance traveled would be $2L$ = (AC + CE), which is predicted by the center movements. However, the centroid displacement, $L' = (AF + FE)$ is less than $2L$, thus resulting in an underestimate of velocity by the following percentage: ERROR = $(-100)*[1 - (L'/2L)]$. This function is calculated for various turning angles and plotted as a dashed curve. If the motion through the turn could be tracked with high time resolution, then L' is approximated by $(AB + BF + FD + DE)$ with error predicted by the solid curve with the simplified equation ERROR = $(-25)*[1 - \sin(90° - (\theta/2))]$.

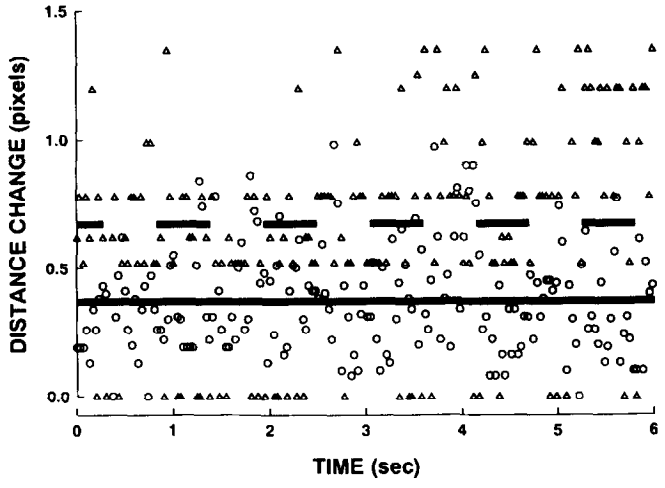

FIG. 6. Accuracy in measuring a stationary actin filament using either the manual (△) or the computer-assisted tracking routine (○). An actin filament was allowed to attach to skeletal muscle myosin (250 μg/ml) in the absence of MgATP. Under these rigor conditions, the filament appears rigidly bound to myosin. The change in position for the filament's centroid between 180 consecutive video frames was determined. The means for the manual (dashed line) and computer-assisted approach (solid line) are shown. Note the discrete changes in filament position associated with the manual approach; see text for details.

short actin filaments, where all results (Figs. 6–9) were obtained using the centroid determination.

ANALYZE—Filament Motion Path Construction

To match filament images between boxes, filament dimensional characteristics and position within the box image are compared. The more similar these attributes, the greater the likelihood that the images being compared are in fact the same filament. A total correlation factor (TCF) between filament images that ranged between 0 and 1 was defined, with 1 a perfect match although 0.5 was considered sufficient. The dimensional and positional attributes used to calculate the TCF were (1) filament pixel area (A), (2) filament major to minor axis length ratio (LR), (3) centroid/center displacement between boxes (CD), and (4) a user-defined maximum travel distance between box images (dX), with the following formula used,

$$\mathrm{TCF} = \frac{(W_a{*}\mathrm{DCF}_a + W_b{*}\mathrm{DCF}_b + W_c{*}\mathrm{DCF}_c)}{(W_a + W_b + W_c)},$$

where W_x are user-defined weighting factors and DCF_x are dimensional correlation factors, with

$$\mathrm{DCF}_a = [1.0 - \min(\mathrm{abs}(A_i - A_{i+1})/A_i, 1.0)]$$

$$\mathrm{DCF}_b = [1.0 - \min(\mathrm{abs}(\mathrm{LR}_i - \mathrm{LR}_{i+1})/\mathrm{LR}_i, 1.0)]$$

$$\mathrm{DCF}_c = [1.0 - \mathrm{CD}/dX].$$

We have empirically identified a set of weighting factors and dX values that operate best under most experimental conditions. The most commonly used parameters are W_a, 35; W_b, 20; W_c, 10; dX, 10 pixels. However, under conditions where filament images are faint or photobleach significantly, the weighting factor for centroid/center displacement should be increased relative to the other dimensional attributes, since centroid/

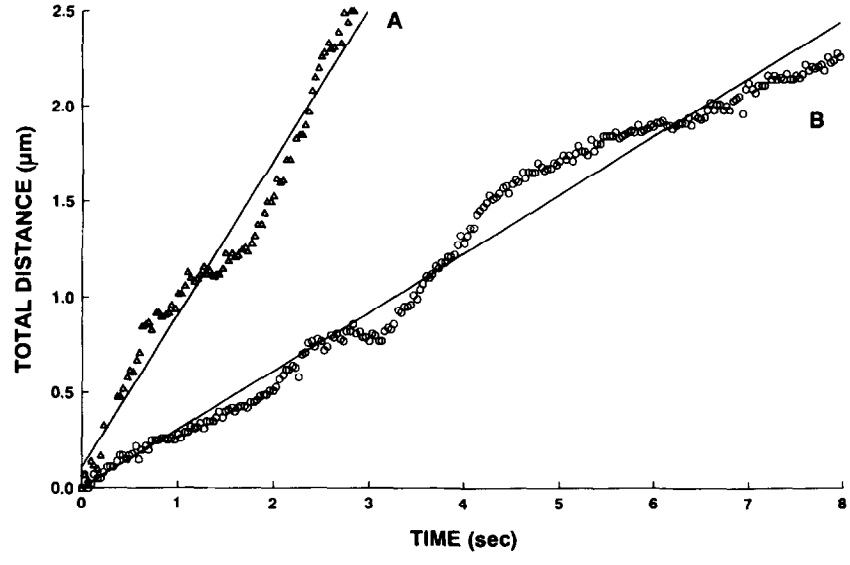

FIG. 7. Distance traveled versus time for actin filament sliding over thiophosphorylated smooth muscle myosin. The motion of two actin filaments was analyzed on a frame by frame basis with 33 ms time resolution. Linear regressions are drawn through the data, thus estimating velocities of 0.80 μm/s for filament A (△) and 0.31 μm/s for filament B (○). The difference in velocities was a result of differences in the experimental conditions.

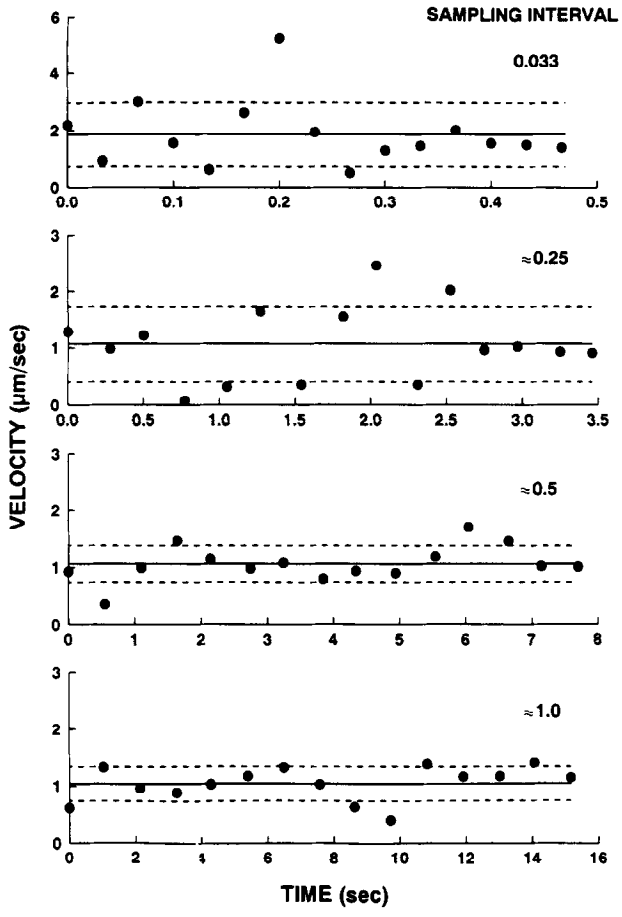

FIG. 8. Incremental velocity versus time profiles for varying sampling intervals. For filament A in Fig. 7, 15 consecutive box images were digitized at four different sampling intervals as indicated in figure. Incremental velocities were calculated between images (see text for details). The mean (solid line) and ±1 SD (dashed lines) are shown for each profile. Note that the standard deviation increases as the sampling interval decreases. The *y* axis on the upper plot is three times greater than the others. The times on the *x* axis differ due to the different sampling intervals.

center position is less affected by photobleaching if it occurs uniformly over the filament.

To begin tracking filament motion, filament images in the first and second boxes are compared using the TCF, with a match creating a filament path. Using the last filament image in a path, comparisons are then made to filament images in the next box until no further matches are obtained, at which time the path is terminated. Premature termination can occur, for example, when filaments cross paths, and the filament image no longer matches any previous image. Once the filaments become distinct after crossing, they then are assigned to a new path and tracked for the remaining boxes. Upon completion of this process, all paths are scanned to identify complete paths, defined as a path spanning 75% of the box images. Any remaining paths are linked by calculating a TCF for the filament image at the end of one path compared to the filament image at the beginning of another path. Once the linking of paths is complete, any path length below a user-defined minimum travel distance is eliminated and the filament is considered stationary.

XVIEW—Filament Velocity Calculation Program

To calculate filament velocity, an interactive program (XVIEW) that allows the user to review each computer identified path is run. The filament images are magnified twofold and displayed on a video monitor with the centroid/center marked by a cross (see Fig. 5). The user advances through each box to accept or reject the computer's tracking efforts. Rejection is necessary if the computer jumps to a neighboring filament. The user would then skip to the next box or manually enter the estimated centroid/center position with a mouse. Once a path is accepted, an incremental velocity versus time profile is calculated from the change in centroid/center position divided by the change in time between boxes. The results are displayed on the video monitor. The user has the final option of implementing a high- and low-velocity cutoff to eliminate any velocity data that do not fit certain criteria. For example, if the user wants velocity data only during times that the filament moves, a low-velocity cutoff can be set to eliminate velocities below the minimum detectable value. Once any velocity cutoffs have been set, the computer displays the filament's mean velocity and standard deviation superimposed on the velocity:time profile and writes the information to a file.

XVIEW also allows the user to manually track filament paths by recalling digitized box images generated in SWEEP. The user tracks filament motion by marking the filament's position on the video monitor with the use of a mouse and velocities calculated as described above. Due to the discrete nature of the video board, the user's ability to define a precise location on the video monitor is restricted to within 1 pixel (see Fig. 6).

Other options are: (1) generation of a composite video image showing the filament's entire path (see Fig. 2C) and (2) identification of a reference point in each video frame against which visual field motion can be corrected. Conditions under which the entire visual field moves with time have existed. For example, a heated microscope stage used in earlier experiments expanded and contracted during its heating cycles. The stage expansion was detectable at these high magnifications, resulting in visual field motion. The current system employs an oil objective heater (Vermont Technologies), eliminating stage motion.

RESULTS

Manual versus Automated Actin Filament Tracking

To compare the accuracy of the computer-assisted tracking to that of manual filament detection, we devel-

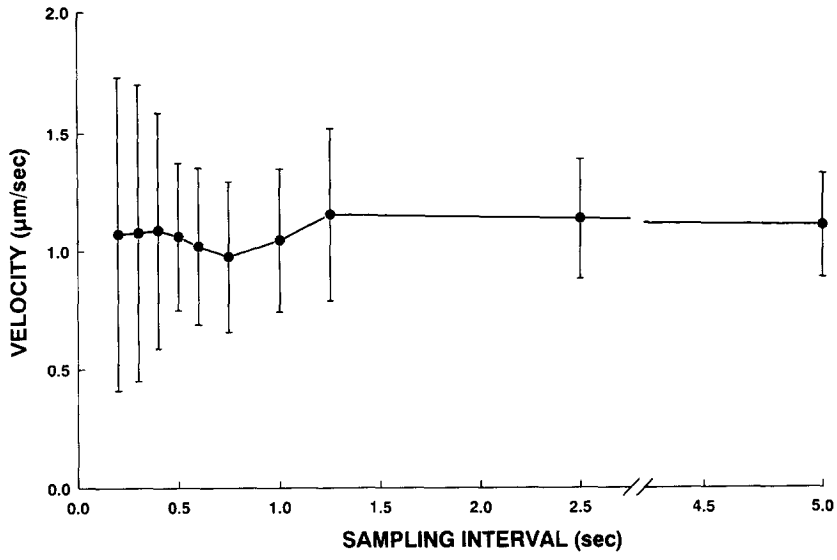

FIG. 9. Actin filament velocity versus sampling interval. (A) The mean and standard deviation in incremental filament velocity for filament A in Fig. 7 are plotted versus different sampling intervals ranging from 0.22 to 5.0 s.

oped a program to generate mock filament images of various shapes and sizes that moved at various velocities on the video monitor. The motion was sinusoidal with variable amplitude and period. Using these computer-generated images, both approaches were within 0.5% of the mock filament velocity over a fivefold range in velocities. In this comparison, the filament images were noise free, whereas real filament images change from frame to frame through slight variations in fluorescence and noise (see Fig. 4). Therefore, the manual and computer-assisted approaches were compared (see Fig. 6) in their ability to identify a stationary filament's position in 180 consecutive video frames (i.e., 6 s). A stationary filament was obtained by allowing actin filaments to bind to high densities of myosin (250 μg/ml) in the absence of MgATP. On average, the user could predict the filament's position to within 0.7 pixels (i.e., 134 nm), half as accurate as the computer (i.e., 67 nm).

Actin Filament Velocity—Effect of Sampling Rate

In Fig. 7, the total distance traveled versus time is plotted for two filaments having velocities that differ by a factor of 2.5. The data were obtained from consecutive video frames (i.e., 33 ms resolution) and linear regressions drawn. These filaments do not travel at a uniform speed but exhibit hesitations and accelerations. Mean velocity and motion characterization data (e.g., percentage time moving) can be readily extracted. Since the single-frame analysis generates large data sets, it is impractical for analyzing experiments with numerous experimental conditions. Therefore, we routinely decrease the sampling rate, knowing that information between grabs is lost and could result in inaccurate estimates of filament velocity (see Discussion). However, for filaments moving at a constant rate, the reduced sampling rate provides a faster approach to data acquisition and analysis.

In Fig. 8 the incremental velocity versus time plots for filament A in Fig. 7 but at different sampling intervals are given. Note that at short sampling intervals (i.e., 0.033 s), the variability in the data can be substantial but diminishes with increased sampling interval. This is evident in the plot of the velocity means and standard deviations for the various sampling intervals (see Fig. 9). The increased variance in velocity at short sampling intervals is a combination of the fixed precision in filament centroid determination (Fig. 6) with additional error due to biologically based fluctuations in the filament image (e.g., myosin derived). Sampling interval must be varied between experimental conditions so that the velocity variance is minimized. An optimum sampling interval is one that gives a standard deviation less than 20% of the mean velocity estimate. In more practical terms, the sampling interval is chosen so that a filament moves by half its length between box images.

DISCUSSION

Actin filament movement in the *in vitro* motility assay is believed to be derived from motion-generating events within the myosin molecule. The most basic question yet to be answered is the amount of motion that a myosin motor imparts to actin per ATP hydrolyzed (1,5,6). To address this question, the true sliding velocity of actin filaments over myosin must be determined. However, the video recording of actin filament motion is quite variable, being subject to inhomogeneities in the density of myosin molecules on the coated surface, interaction of actin with nonfunctional myosin motors,

Brownian motion, and video system noise. These factors, as well as the accuracy of the methodology used to track actin filament motion, contribute to errors in estimating actin filament position and should be considered before conclusions about molecular mechanisms are made.

Earlier versions of the motility assay were performed by monitoring the movement of myosin-coated polystyrene beads over actin cables of the algae *Nitella* (10). Initially, bead motion was detected manually by tracing the bead path on plastic wrap placed over the video monitor (11). A computer-assisted approach in which the bead center was marked on the monitor using a trackball in combination with the cursor keys was developed (11). This computer-assisted approach is similar to the manual approach that we describe above for tracking actin filaments. More recently, Gelles *et al.* (9) greatly improved the spatial resolution of bead tracking to within 1–2 nm by a statistical analysis of digitized video bead images. Although highly accurate, this approach relies on a cross-correlation between relatively reproducible bead images and thus does not lend itself to tracking actin filaments, where filament images vary dramatically in time (Fig. 4).

Actin filament tracking can now be performed using commercially available computer-assisted tracking systems (Celltrak, Motion Analysis Corp.) or image analysis software (12). These tracking routines and that described here rely on digital image processing and pattern recognition algorithms (13,14) and are susceptible to errors in estimating filament velocity. However, with knowledge of the error source and definable program parameters, errors in velocity can be minimized.

The accuracy in determining the filament centroid and its use for long filaments rather than the filament center contribute to errors in actin filament velocity. As described under Methods and Results, actin filament images can be difficult to visualize (i.e., lack of contrast) and are visually modified by recording system noise and photobleaching. In addition, actin filaments are flexible structures that are responsive to the physical forces applied [(15); see Discussion above)] and, as a result, commonly travel along serpentine paths. One can readily calculate the extent to which actin filament velocity will be underestimated for filaments that turn during their motion rather than move along a straight path (see Fig. 5). As a filament turns, its centroid is off the filament and the centroid velocity will underestimate the true filament velocity by as much as 25% depending on the turning angle and the total distance traveled in the turn. To avoid this error, one can choose only to analyze short filaments or long filaments that travel along a straight path. Our approach for long filaments has been to develop a computer algorithm that identifies the filament center rather than centroid, thus reducing the error associated with turning filaments (see Methods).

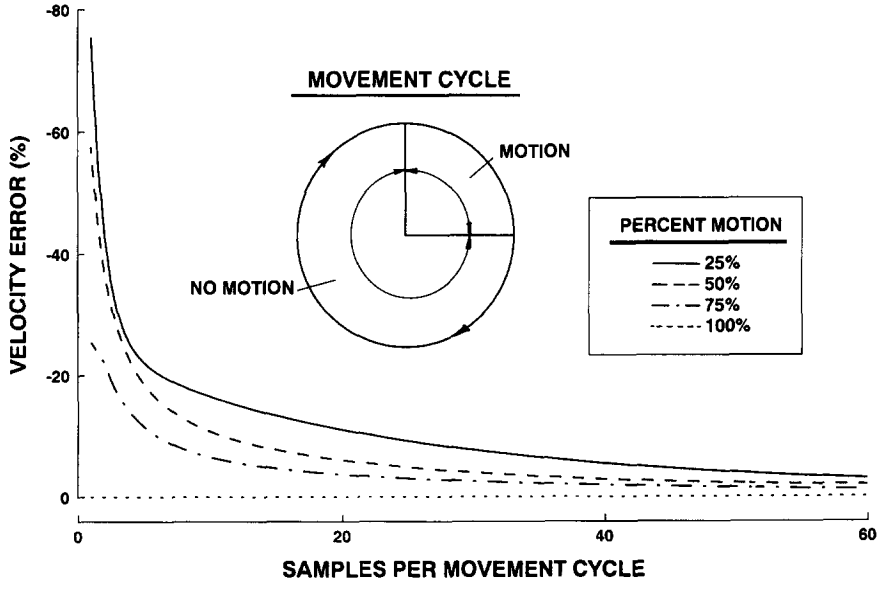

FIG. 10. Estimated velocity error for sporadically moving filament. If an actin filament does not move continuously, then one can derive a simplified equation that relates the velocity error to the sampling rate and fractional time of filament motion. Let us define a movement cycle, consisting of stationary periods and periods of motion, with motion occurring for a fraction (f) of the cycle. To accurately estimate velocity, the number of samples per movement cycle (S) should be great enough that stationary periods can be resolved. Regardless of the sample number, there will be at least one sample and probably more that span the transition between motion and the stationary period. The velocity associated with these samples would be less than the true filament velocity when moving. If these velocity data are averaged with the other samples that accurately record filament velocity when it occurs, then the true velocity will be underestimated by ERROR = $(-100)*[1 - (f*S)/\text{ROUNDUP}(f*S)]$. The results of this theoretical treatment are shown for varying percentages of motion within the movement cycle and samples per movement cycle.

The choice of sampling interval between frames is another major source of error. The accuracy in estimating the incremental actin filament velocity between frames is reduced as the sampling interval is diminished (see Figs. 8 and 9). This would not pose a significant problem for actin filaments that move continuously and do not stop during the observation period. However, sporadically moving actin filaments that hesitate do exist. These hesitations are either biologically important given the experimental conditions or due simply to inhomogeneities in the myosin-coated surface. Regardless, the true filament velocity while moving would be underestimated if the sampling interval were too long to resolve stationary periods. Therefore it is necessary to characterize the fractional time that filaments move and their average movement cycle time. Note that by movement cycle we are not referring to the inherent actomyosin ATPase cycle but rather to a grosser movement phenomenon. From a theoretical treatment (see Fig. 10 and legend), it is obvious that the highest sampling rate should be used to reduce error. However, high sampling rates and the fixed precision in centroid determination contribute to significant velocity errors if calculated between frames. One approach to minimize the error associated with high sampling rates is to average over many frames (see Fig. 7).

To date, the assumption has been that video-based tracking is sufficient to accurately measure actin filament velocity. It is conceivable, however, that even at these video frame rates (i.e., 30 frames or 60 fields per second), the sampling rate is too slow to resolve the filament's fractional motion time. Thus, actin filament velocities could be greatly underestimated. Investigators should be concerned with this possible error before actin filament velocity is used as evidence to support hypotheses regarding the molecular mechanism underlying actin-based motility. In the future, non-video-based tracking systems may be developed with both high time and spatial resolution, which may help improve the accuracy in estimating actin filament velocity.

ACKNOWLEDGMENTS

We thank both Pat Urban and Daniel Taugas at Coreco Inc. for their assistance and helpful discussions in our design of the pattern recognition software. We thank K. Trybus, D. Harris, and J. Desrosiers for their comments on this manuscript. This work was supported by funds from the National Institutes of Health (Grants AR34872 and HL45161 to D.M.W. and HL28001 to N. R. Alpert) D.M.W. is an Established Investigator of the American Heart Association.

REFERENCES

1. Huxley, A. F. (1980) Reflections on Muscle, Princeton Univ. Press, Princeton, NJ.
2. Taylor, E. W. (1979) *CRC Crit. Rev. Biochem.* **4,** 103–164.
3. Kron, S. J., and Spudich, J. A. (1986) *Proc. Natl. Acad. Sci. USA* **83,** 6272–6276.
4. Harada, Y., Noguchi, A., Kishino, A., and Yanagida, T. (1987) *Nature* **326,** 805–808.
5. Uyeda, T. Q. P., Warrick, H. M., Kron, S. J., and Spudich, J. A. (1991) *Nature* **352,** 307–311.
6. Harada, Y., Sakurada, K., Aoki, T., Thomas, D. D., and Yanagida, T. (1990) *J. Mol. Biol.* **216,** 49–68.
7. Warshaw, D. M., Desrosiers, J. M., Work, S. S., and Trybus, K. M. (1990) *J. Cell Biol.* **111,** 453–463.
8. Tawada, K., and Sekimoto, K. (1991) *Biophys. J.* **59,** 343–356.
9. Gelles, J., Schnapp, B. J., and Sheetz, M. P. (1988) *Nature* **331,** 450–453.
10. Sheetz, M. P., and Spudich, J. A. (1983) *Nature* **303,** 31–35.
11. Sheetz, M. P., Block, S. M., and Spudich, J. A. (1986) *in* Methods in Enzymology (Vallee, R. B., Ed.), Vol. 134, pp. 531–544, Academic Press, Orlando, FL.
12. Soll, D. R. (1988) *Cell Motil. Cytoskel.* **10,** 91–106.
13. Kovalevsky, V. A. (1980) Image Pattern Recognition, Springer-Verlag, New York.
14. Gonzalez, R. C., and Wintz, P. (1977) Digital Image Processing, Addison-Wesley, Reading, MA.
15. Yanangida, T., Arata, T., and Oosawa, F. (1985) *Nature* **316,** 366–369.